

NRC Publications Archive Archives des publications du CNRC

Theoretical analysis on spatially structured beam induced mass transport in azo-polymer films

Ferrer-Garcia, Manuel F.; Alvandi, Yousef; Zhang, Yingwen; Karimi, Ebrahim

This publication could be one of several versions: author's original, accepted manuscript or the publisher's version. / La version de cette publication peut être l'une des suivantes : la version prépublication de l'auteur, la version acceptée du manuscrit ou la version de l'éditeur.

For the publisher's version, please access the DOI link below. / Pour consulter la version de l'éditeur, utilisez le lien DOI ci-dessous.

Publisher's version / Version de l'éditeur:

<https://doi.org/10.1364/OE.395054>

Optics Express, 28, 14, pp. 19954-19965, 2020-07-06

NRC Publications Archive Record / Notice des Archives des publications du CNRC :

<https://nrc-publications.canada.ca/eng/view/object/?id=6ad08191-c968-43b4-8222-8d636e0b6046>

<https://publications-cnrc.canada.ca/fra/voir/objet/?id=6ad08191-c968-43b4-8222-8d636e0b6046>

Access and use of this website and the material on it are subject to the Terms and Conditions set forth at

<https://nrc-publications.canada.ca/eng/copyright>

READ THESE TERMS AND CONDITIONS CAREFULLY BEFORE USING THIS WEBSITE.

L'accès à ce site Web et l'utilisation de son contenu sont assujettis aux conditions présentées dans le site

<https://publications-cnrc.canada.ca/fra/droits>

LISEZ CES CONDITIONS ATTENTIVEMENT AVANT D'UTILISER CE SITE WEB.

Questions? Contact the NRC Publications Archive team at

PublicationsArchive-ArchivesPublications@nrc-cnrc.gc.ca. If you wish to email the authors directly, please see the first page of the publication for their contact information.

Vous avez des questions? Nous pouvons vous aider. Pour communiquer directement avec un auteur, consultez la première page de la revue dans laquelle son article a été publié afin de trouver ses coordonnées. Si vous n'arrivez pas à les repérer, communiquez avec nous à PublicationsArchive-ArchivesPublications@nrc-cnrc.gc.ca.



Theoretical analysis on spatially structured beam induced mass transport in azo-polymer films

MANUEL F. FERRER-GARCIA,^{1,4}  YOUSEF ALVANDI,^{1,2,4} YINGWEN ZHANG,³ AND EBRAHIM KARIMI^{1,2,3,*} 

¹Physics Department, University of Ottawa, Advanced Research Complex, 25 Templeton, Ottawa, ON K1N 6N5, Canada

²Department of Physics, Institute for Advanced Studies in Basic Sciences, Zanjan 45137-66731, Iran

³National Research Council of Canada, 100 Sussex Drive, Ottawa, ON K1A0R6, Canada

⁴These authors contributed equally to this work

*ekarimi@uottawa.ca

Abstract: The radiation force from paraxial beams possessing helical phase fronts causes twists on the surface of an azobenzene polymer sample, and leads to the formation of micro-scale structures. Here, we theoretically investigate the radiation force generated by spatially structured optical beams on a dispersive-absorptive substrate. We derive an analytical expression for the radiation force from spatially structured polarized beams, including, lemon, star, monstar and vector vortex beams in the paraxial regime. Finally, we extend our calculation for non-paraxial beams - optical beams under the tight-focusing regime - and simulate the transverse radiation forces numerically at the focal plane.

© 2020 Optical Society of America under the terms of the [OSA Open Access Publishing Agreement](#)

1. Introduction

Structured light - electromagnetic waves possessing well-engineered amplitude, polarization, and spatial modes - has received increasing interest during the last few decades [1,2]. For instance, beams carrying orbital angular momentum (OAM) have been used in optical microscopy (ranging from optical spanners to stimulated emission depletion microscopy) [3,4], telecommunications [5–8] and quantum information [9,10]. The interaction of structured light beams and their induced optical forces for beams, such as Bessel beams [11–13] Airy beams [13,14], Airy sheets [15] and Poincaré beams [16,17], have been widely explored with very promising results during the last decades. Very recently, the interaction between spatially structured optical beams and an a medium with complex electrical susceptibility has been studied at the quasi-continuous wave (CW), pico-, nano- and femtosecond regimes [18–22].

Among all the possible materials, azo-polymers - organic polymers containing azo functional groups - have recently attracted much attention from the scientific community due to the exhibited reversible photo-induced isomerization [23]. It has been shown that a photoinduced mass transport phenomena is triggered when an azo-polymer film is illuminated with light in the ultraviolet or visible wavelengths, leading to controlled deformations on the polymer film [24–27]. Such modifications of the surface relief has been proven to be wavefront-sensitive [28]. In particular, it has been shown that beams carrying optical angular momentum (spin and OAM) can induce mass-transport and produce nano-scale helical structures [29–32]. Nevertheless, since the isomeric transitions are reversible, this photoinduced writing can be erased by heating or irradiating the sample with incoherent light [33]. This photoresponsive property makes the azo-polymers highly suitable for multiple applications, such as reversible storage materials, holographic gratings and micro-scale machining [25,33–36]. A simple analytical approach for the photoinduced surface relief formation based on the macroscopic optical radiation force by a

continuous-wave vortex beam was used to explain the spiral shaped deformations formed in the azo-polymer film in paraxial approximation [31].

Here, we extend this analysis from vortex beams to space-varying polarized light beams. The induced-force density due to structured optical beams onto the surface of a dispersive-absorptive medium is calculated at both paraxial and non-paraxial regimes. First, we present the calculations for the coherent superposition of optical vortices having opposite polarization states, e.g. the Cylindrical (CV) Vector beams [37] and the Full-Poincaré (FP) beams (including lemon, star and monstar polarization topologies) [38]. We have allocated the optical properties of an arbitrary azo-polymer in our calculations. Later on, a numerical analysis for the non-paraxial case of tightly focused vector beams is provided. Due to the combination of the inhomogeneous polarization and phase distributions, we predict the possible formation of significantly more complex patterns on the azo-polymer.

2. Optical forces due to structured light

The time-averaged optical radiation force density \mathbf{F} , which arises from optically induced electric polarization in a dielectric material, is expressed as, [31]

$$\mathbf{F} = \langle \rho_p \mathbf{E} + \mathbf{j}_p \times \mathbf{B} \rangle, \quad (1)$$

where \mathbf{E} and \mathbf{B} are respectively the electric field and magnetic flux density, ρ_p is the polarization charge density, \mathbf{j}_p is polarization current density, and $\langle \cdot \rangle$ stands for time-average. For an isotropic and homogeneous material, such as azo-polymers when they are illuminated with a low power source, the surface polarization charge density is equal to zero ($\rho_p = 0$), and the polarization current density (for a monochromatic beam) can be written as $\mathbf{j}_p = -i\omega\epsilon_0\chi\mathbf{E}$. Here, ϵ_0 is the dielectric constant in vacuum, ω is the angular frequency of the optical field, and $\chi = \chi_r + i\chi_i$ is the complex electric susceptibility of the material. Therefore, Eq. (1) can be expressed as,

$$\begin{aligned} \mathbf{F} &= \langle i\omega\epsilon_0\chi\mathbf{E} \times \mathbf{B} \rangle \\ &= \frac{\omega\epsilon_0}{2} [\chi_r \text{Im}(\mathbf{E} \times \mathbf{B}^*) + \chi_i \text{Re}(\mathbf{E} \times \mathbf{B}^*)]. \end{aligned} \quad (2)$$

Here, the first term that is proportional to χ_r is a scattering force, while the second term which is proportional to χ_i is related to the absorption. Note that for the sake of simplicity, we have considered monochromatic electric fields with frequency ω . Using the Maxwell-Faraday equation, which dictates the relationship between the magnetic density flux and the electric field, i.e. $\mathbf{B} = (-i/\omega)\nabla \times \mathbf{E}$, Eq. (2) yields,

$$\mathbf{F} = \frac{\epsilon_0}{2} [-\chi_r \text{Re}(\mathbf{E} \times \nabla \times \mathbf{E}^*) + \chi_i \text{Im}(\mathbf{E} \times \nabla \times \mathbf{E}^*)], \quad (3)$$

in which the time-averaged optical radiation force is expressed in terms of just the electric field and properties of the materials. It should be noted that Eq. (3) is a general expression for the optical force when an arbitrary electromagnetic field (with electric field \mathbf{E}) illuminates an azo-polymer film. The complex electric susceptibility $\chi = \chi_r + i\chi_i$ can be obtained from the transmission spectrum and Kramers-Kronig relations [39].

For the specific case of structured light, we consider an electric field formed by the coherent superposition of two optical vortices having opposite circular polarization states, i.e.,

$$\mathbf{E} = \mathbf{E}_1 + \mathbf{E}_2 = \left[\cos \alpha \text{LG}_{p_1}^{\ell_1}(r, \phi) \hat{\mathbf{e}}_{\mathbf{R}} + e^{i\delta} \sin \alpha \text{LG}_{p_2}^{\ell_2}(r, \phi) \hat{\mathbf{e}}_{\mathbf{L}} \right] e^{ikz}, \quad (4)$$

where $\{\hat{\mathbf{e}}_{\mathbf{R}}, \hat{\mathbf{e}}_{\mathbf{L}}\}$ are unit vectors of the circular polarization basis, and $k = 2\pi/\lambda$ is the wavenumber. The relative amplitude and phase between both beams can be tuned by the parameters $\alpha \in [0, \pi/4]$

and $\delta \in [0, 2\pi]$, respectively. The normalized amplitude of the optical vortices in cylindrical coordinates (r, ϕ, z) at a given plane (plane of interaction, i.e. $z = 0$) is described by Laguerre-Gauss (LG) modes,

$$\text{LG}_p^\ell(r, \phi) = \sqrt{\frac{2(p!)^2}{\pi(p + |\ell|)! w_0}} \left(\frac{\sqrt{2}r}{w_0}\right)^{|\ell|} L_p^{|\ell|} \left(\frac{2r^2}{w_0^2}\right) \exp\left(-\frac{r^2}{w_0^2}\right) e^{i\ell\phi}, \quad (5)$$

where w_0 is the waist of the Gaussian envelope at the plane $z = 0$, $L_p^{|\ell|}(\cdot)$ is the generalized Laguerre polynomials with azimuthal and radial indices of ℓ and p , respectively. The field described by Eq. (4) allows us to produce spatially variant polarization patterns, which are characterized by the topological index of the polarization singularity η [40]. η , the polarization topological index, is the amount of rotation of the polarization ellipse in a closed path around a point of circular polarization divided by 2π , and its quantity for a continuous field is half-integer. It is easy to show that Eq. (3), the induced force density, can now be written as

$$\mathbf{F} = \frac{\epsilon_0}{2} \left[-\chi_r \text{Re} \left(\sum_{i,j} \mathbf{E}_i \times \nabla \times \mathbf{E}_j^* \right) + \chi_i \text{Im} \left(\sum_{i,j} \mathbf{E}_i \times \nabla \times \mathbf{E}_j^* \right) \right]. \quad (6)$$

The vector quantity in Eq. (6), i.e. $\mathbf{E}_i \times \nabla \times \mathbf{E}_j^*$, is given by,

$$\begin{aligned} \mathbf{E}_i \times \nabla \times \mathbf{E}_j^* &= \frac{a_i a_j e^{i\delta_{ij}} \text{LG}_{p_i}^{\ell_i}(r, \phi)}{2} \\ &\times \left\{ e^{-i\sigma_j \phi} \left[\frac{l_j}{r} \text{LG}_{p_j}^{-\ell_j}(r, \phi) + \sigma_j \frac{\partial}{\partial r} \left(\text{LG}_{p_j}^{-\ell_j}(r, \phi) \right) \right] (-i\sigma_i \hat{\mathbf{x}} + \hat{\mathbf{y}}) \right. \\ &\quad \left. - ik \text{LG}_{p_j}^{-\ell_j}(r, \phi) (\sigma_i \sigma_j + 1) \hat{\mathbf{z}} \right\}, \end{aligned} \quad (7)$$

where $a_{i(j)}$ are superposition weights (i.e. $\cos \alpha$ and $\sin \alpha$), $\sigma_{i(j)} = \pm 1$ are the beams' helicities, and δ_{ij} is the relative phase between \mathbf{E}_i and \mathbf{E}_j .

For simplicity we assume LG modes with zero radial index, i.e. $p = 0$. Intensity of these beams is characterized by a single-ring shape (e.g., see Fig. 1), and it is invariant under free-space propagation. The above expression for LG modes with $p = 0$ reads,

$$\begin{aligned} \mathbf{E}_i \times \nabla \times \mathbf{E}_j^* &= \frac{a_i a_j e^{i\delta_{ij}} \text{LG}_0^{\ell_i}(r, \phi) \text{LG}_0^{-\ell_j}(r, \phi)}{2} \\ &\times \left\{ e^{-i\sigma_j \phi} \left[\frac{\ell_j + \sigma_j |\ell_j|}{r} - \frac{2\sigma_j r}{w_0^2} \right] (-\sigma_i \hat{\mathbf{x}} + \hat{\mathbf{y}}) - ik(\sigma_i \sigma_j + 1) \hat{\mathbf{z}} \right\}. \end{aligned} \quad (8)$$

It should be noted that the optical radiation force density in the the transverse plane varies slowly upon propagation – this can be seen in Eq. (4), where the field varies slowly in z , i.e. paraxial approximation. The previous expression can be substituted in Eq. (6) to obtain an analytical expression for the force density. Numerical simulations are used to calculate the optical radiation forces exerted on an azo-polymer film substrate. In these simulations, we assume the incident beam carries low power (below <50 mW), and an optically linear substrate where $\chi_r \approx \chi_i$ are constant for a certain wavelength in the visible domain. As a first example, we consider the exerted force for the CV beams, which are recovered from Eq. (4), when one sets $\alpha = \pi/4$ and

$\ell_1 = -\ell_2 = \ell$ for non-zero ℓ s, i.e.,

$$\mathbf{E}_{\text{CV}} = \left(\frac{1}{\sqrt{2}} \text{LG}_0^\ell(r, \phi) \hat{\mathbf{e}}_{\mathbf{R}} + \frac{e^{i\delta}}{\sqrt{2}} \text{LG}_0^{-\ell}(r, \phi) \hat{\mathbf{e}}_{\mathbf{L}} \right) e^{ikz}. \quad (9)$$

The intensity of these beams is a doughnut shape with a space-varying linear polarization. The orientation of the linear polarization on the intensity ring changes azimuthally, and it possesses a topology with $|\ell|$ -fold symmetry, here ($|\eta| = 1$). Intensity and polarization distributions for two classes of the CV beams are shown in Figs. 1 and 2 - see bottom row. The transverse optical force density for these two beams, using Eq. (3), is calculated and shown in the upper row of Figs. 1 and 2. It can be noted that the absorption-dependent contribution, of the force vanishes for every value of ℓ . Furthermore, it is evident that for the case of a radially polarized light, the optical force density only exists in the z -direction, as seen in the first column of Fig. 1 - the force density does not have transverse components. In particular, for the case of $\ell = 1$ as the value of δ reaches to π , the magnitude of the exerted force on the surface increases independently of the polymer's absorption. The magnitude of the optical radiation force vanishes in the presence of polarization dislocations, creating a $2|\ell - 1|$ petal-like pattern in Fig. 2. Variations in the relative phase between the beams induce a rotation on the local polarization ellipse, as it can be observed in Figs. 1 and 2. Moreover, for positive values of ℓ , the force lines point towards the vortex singularity, and this direction is inverted when the topological charge is negative. Following these results, it is evident that the use of CV beams in the formation of complicated landscapes on the surface of an azo-polymer film independently of the absorption coefficient is possible.

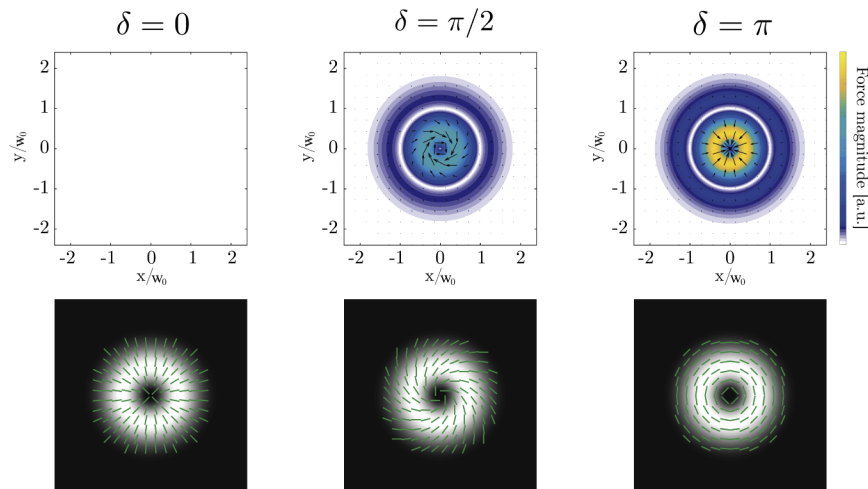


Fig. 1. Transverse optical radiation force density of a CV beam with $\ell = 1$ for $\delta = 0, \pi/2, \pi$. The colormap indicates the force magnitude, whereas the arrows indicate the force direction. The lower row shows the corresponding polarization distribution and intensity profile over the beam's transverse plane.

In a similar fashion, the induced optical radiation force is calculated for another set of space-varying polarized beams: Full-Poincaré (FP) beams [38]. In contrast with the CV beams, the polarization distribution of FP beams spans the entire surface of the Poincaré sphere while the beams' intensity is a quasi-uniform (flat-top) profile - see the first column of Fig. 3(a), (b), (c). Two possible types of polarization dislocations with non-integer η arise from Eq. (4): lemon and star topologies. However, a hybrid, nevertheless, independent topology, called monstar, can be

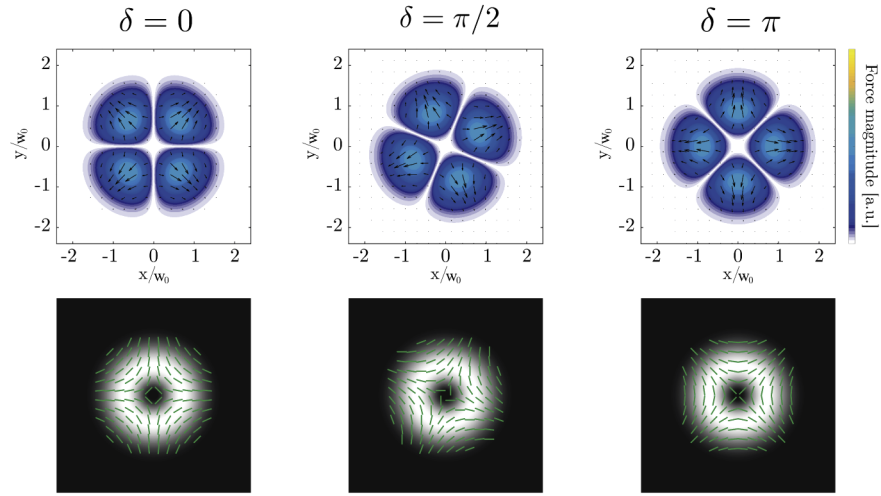


Fig. 2. Transverse optical radiation force density of a CV beam with $\ell = -1$ for various values of $\delta = 0, \pi/2, \pi$. The colormap indicates the force magnitude, whereas the arrows indicate the force direction. The lower row shows the corresponding polarization distribution over the intensity profile.

obtained when a third optical vortex is added to, Eq. (4) [41,42]

$$\mathbf{E}_{\text{FP}} = \left\{ \cos \alpha \left[\cos \beta \text{LG}_0^{\ell_1}(r, \phi) - \sin \beta \text{LG}_0^{-\ell_1}(r, \phi) \right] \hat{\mathbf{e}}_{\mathbf{R}} + e^{i\delta} \sin \alpha \text{LG}_0^{\ell_2}(r, \phi) \hat{\mathbf{e}}_{\mathbf{L}} \right\} e^{ikz}, \quad (10)$$

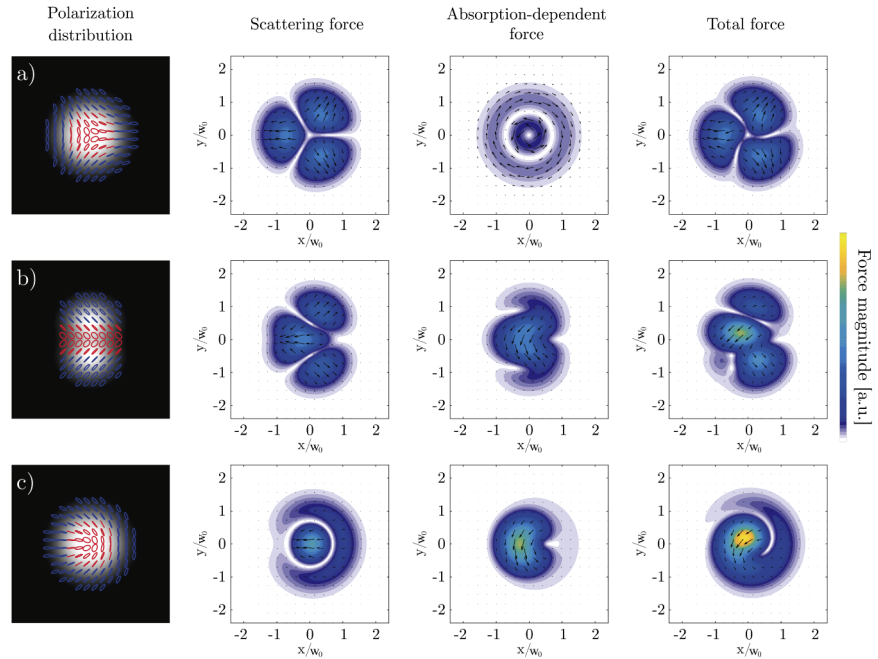


Fig. 3. Transverse optically induced force density of FP beams for (a) star ($\beta = 0$), (b) monstar ($\beta = \pi/4$), and (c) lemon ($\beta = \pi/2$) polarization topologies. The colormap indicates the force magnitude, whereas the arrows indicate the force direction. The first column shows the corresponding polarization distribution over the intensity profile. The red and blue colors of the ellipses indicate their handedness, left- and right-handed, respectively.

where $\beta \in (0, \pi/2)$. Equation (8) is still valid and can be used to calculate the induced force density. As it is shown in Fig. 3, both the scattering and absorption-dependent force contributions exert a non-trivial effect on the surface relief of the azo-polymer. Notice that the absorption-dependent force density for the star topology is formed by two rings with opposite directions – the force is counterclockwise for inner ring and clockwise for the outer ring. In this case, the induced force contribution is significantly smaller than that exerted by the scattering part. However, this symmetry is broken for any other configuration. In fact, for the case of lemon topology, the contribution due to χ_i , i.e. the absorption force, overcomes the scattering forces.

3. Optical forces of tightly focused space-varying polarized beams

Heretofore, we have considered paraxial beams whose polarization distribution exclusively lies on a transverse plane. However, it is well-known that when optical beams undergo focusing by means of a high numerical aperture (NA) lens, i.e. tight-focusing regime, a longitudinal component of the beam arises [43]. Indeed, the beam wavefront is tilted, and thus the beam polarization (which is locally transverse) possesses a component along the beams propagation direction. Under these conditions, it has been shown that the non-paraxial polarization structure generates complex and exotic 3-dimensional polarization topologies, such as Möbius strips or ribbons [44,45]. As a result of the creation of this non-negligible longitudinal component in the electric field, the cylindrical symmetry of the vector beam's intensity is broken for most of the cases [46] – see Fig. 4(b). Therefore, we present an analysis of the optical force exerted by the space-varying polarized beams, namely those beams studied in the previous section, under tight-focusing regime.

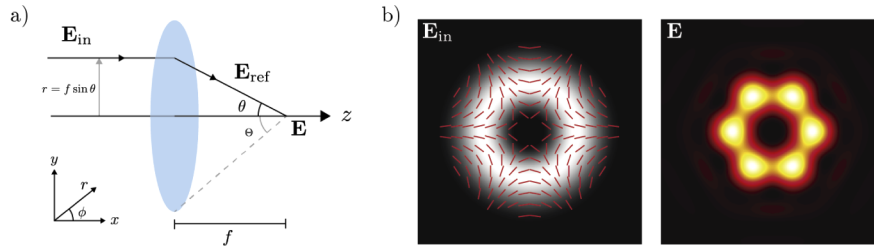


Fig. 4. Tight focusing of optical beams: (a) Schematic diagram of the coordinate system transformation used to calculate the tightly focused fields, (b) Input field and its corresponding focal field distribution intensity.

The electric field $\mathbf{E}_f(\rho, \varphi, z)$ at the focal plane of an aplanatic lens with focal length f , is given by Richards and Wolf's diffraction integral, [47]

$$\mathbf{E}_f(\rho, \varphi, z) = -\frac{ikf}{2\pi} e^{-ikf} \int_0^{2\pi} \int_0^{\Theta} \mathbf{E}_{\text{ref}}(\phi, \theta) e^{ikz \cos \theta + ik\rho \sin \theta \cos(\phi - \varphi)} \sin \theta d\theta d\phi, \quad (11)$$

where $\Theta = \arcsin(\text{NA}/n)$ is the maximum angular aperture of the objective, n is the refractive index of the medium, NA is the lens numerical aperture, and $\mathbf{E}_{\text{ref}}(\theta, \phi) = \mathbf{T} \mathbf{E}_{\text{in}}(\theta, \phi)$ is the transformation of the incident field \mathbf{E}_{in} after the objective, see Fig. 4. The transformation matrix \mathbf{T} for $\mathbf{E}_{\text{in}} = (E_x(\theta, \phi), E_y(\theta, \phi), 0)^T$ - T stands for transpose - is given by,

$$\mathbf{T} = \sqrt{\cos \theta} \begin{bmatrix} -\cos^2 \phi \cos \theta + \sin^2 \phi & -\cos \phi \sin \phi (\cos \theta + 1) & -\cos \phi \sin \theta \\ -\cos \phi \sin \phi (\cos \theta + 1) & \cos^2 \phi - \sin^2 \phi \cos \theta & -\sin \phi \sin \theta \\ \cos \phi \sin \theta & \sin \phi \sin \theta & -\cos \theta \end{bmatrix}. \quad (12)$$

Here, the input field \mathbf{E}_{in} does not have a z -component; however, the transformation matrix \mathbf{T} is given in its general form. It must be noted that despite \mathbf{E}_{in} is a solution to the paraxial equation, \mathbf{E}_{r} satisfies Maxwell's Equations. Since closed analytical solutions for Eq. (11) are hard or even impossible to obtain, the components of the electric field under tight focusing in air ($n = 1$) are calculated by numerical integration of Eq. (11) when the incident field is given by Eq. (4). In addition to the assumptions of the previous section, we consider a microscope objective with $\text{NA} = 0.95$ and the waist of the beam follows the relation $w_0 = f \text{NA}/n$ in order to fill completely the back of the microscope objective. Likewise, very short exposure times have been considered in order to avoid photo-bleaching, substrate degradation or damage due to the high-intensity irradiation.

In order to offer a more complete comparison between the paraxial and non-paraxial regimes, we have performed numerical calculations for the optical induced forces due to tightly focused Laguerre Gauss modes with radial index $p = 0$ and uniform polarization distribution. First, we present the results for an LG_0^0 mode with different polarization states on the Poincaré sphere. The results of numerical calculations are shown in Fig. 5. For a linearly polarized LG_0^0 beam, the induced force is associated to the real part of the electrical susceptibility, i.e. scattering force. The exerted force creates stretching-compressing effects on the surface of the azo-polymer film, whose direction depends on the inclination angle of the linear polarization state of the incident beam \mathbf{E}_{in} . A rotation is induced on the transverse optical radiation force density when

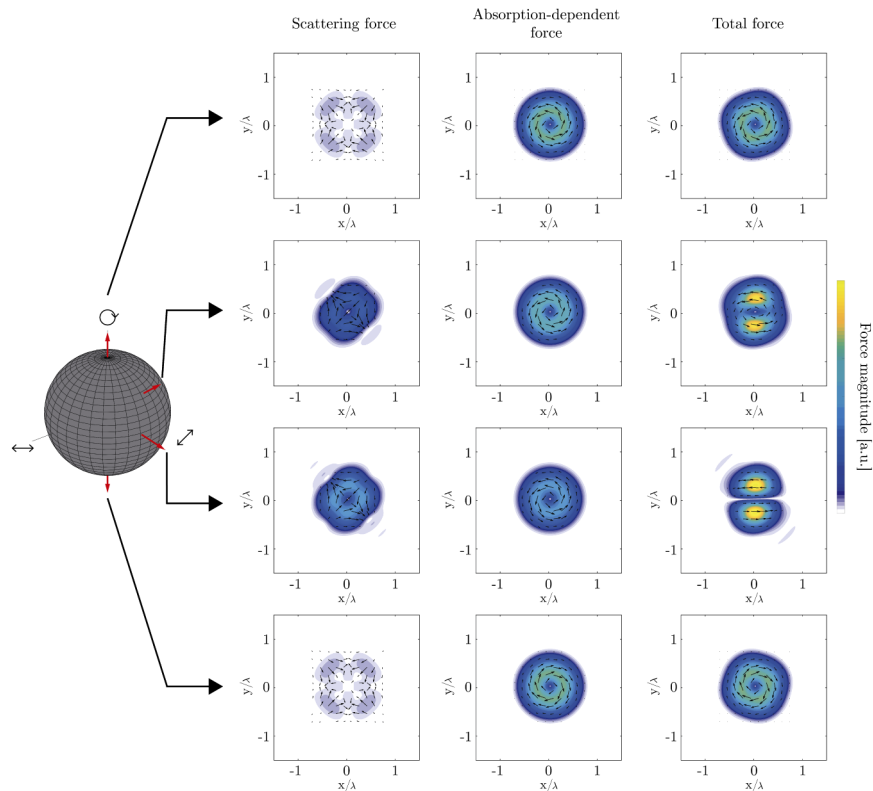


Fig. 5. Transverse optical radiation force density of a tightly focused LG_0^0 beam having different polarization states at the focal plane of an objective lens with numerical aperture of 0.95. The colormap indicates the force magnitude, whereas the arrows indicate the force direction.

the polarization state moves along different latitude lines of the Poincare sphere. By changing the polarization state from linear to elliptical and then to circular - going from equator to poles - an absorption-dependent contribution that is pointing in the azimuthal direction appears. The direction of this force is directly related to the helicity of the polarization state. Moreover, the absorption-dependent force overcomes the scattering force for the case of purely circular polarization states.

Similarly, we numerically calculate the induced optical forces exerted due to a tightly focused LG_0^1 , Laguerre Gauss mode with azimuthal index of +1, when it carries different uniform polarization states. The results of numerical calculations are shown in Fig. 6. In contrast to the previous case, i.e. induced force due to LG_0^0 , an absorption-dependent component of the force in the azimuthal direction exists for the case of a uniform linear polarization. It must be noticed that, as in the case of a fundamental Gaussian beam, the absorption-dependent force overcomes the scattering component for the case of circular polarization. However, the optical radiation force density for both circular polarization states is different due to the generated spin-orbit coupling [48] during the tight focusing process. When the helicity and the topological charge of the optical vortex have the same sign, the direction of the force is uniform in the transverse plane. While, when the signs are opposite to each other, an inversion on the force's direction happens at a certain distance r from the beam axes.

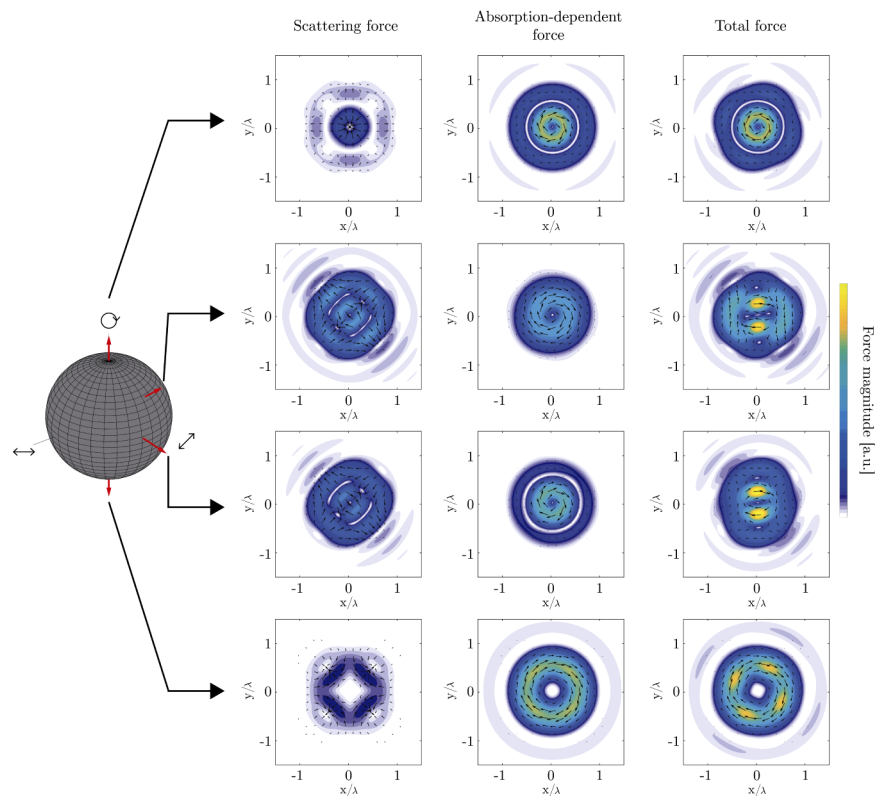


Fig. 6. Transverse optical radiation force density of a tightly focused LG_0^1 beam carrying different polarization states at the focal plane of an objective lens with numerical aperture of 0.95. The colormap indicates the force magnitude, whereas the arrows indicate the force direction.

As a next step, we calculate the induced force density for tightly focused CV beams. The results of numerical simulations are shown in Fig. 7 and Fig. 8 for CV beams with $\ell = 1$ and $\ell = -1$, respectively. As in the paraxial counterpart, see Fig. 1 and Fig. 2, the absorption-dependent contribution is zero for all values of δ . Note that as δ increases, the induced force density in the transverse plane experiences a counter-clockwise rotation of $\delta/2$, while the direction of the force varies according to δ . In particular, the optical radiation force density for $\ell_1 = -\ell_2 = 1$, if formed by two rings with opposite directions, leading to extrusion or compression of the azo-polymer film when $\delta = 0$ and $\delta = \pi$, respectively. During the transition ($0 < \delta < \pi$), the material experiences a torsion, whose direction depends on the sign of δ . It must be noted that the force density of the CV beams exhibits the same type of symmetry as its corresponding intensity distribution.

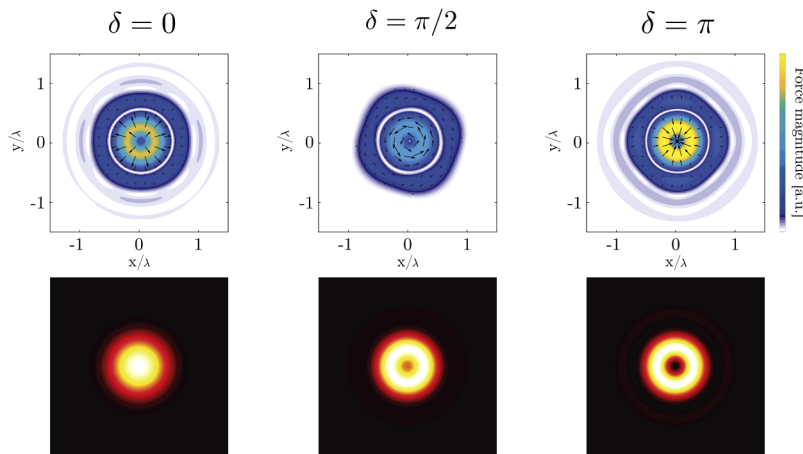


Fig. 7. Transverse optical radiation force density of a tightly focused CV beam with $\ell = 1$ for various values of $\delta = 0, \pi/2, \pi$ at the focal plane. The colormap indicates the force magnitude, whereas the arrows indicate the force direction. The lower row shows the corresponding intensity profile at the focal plane.

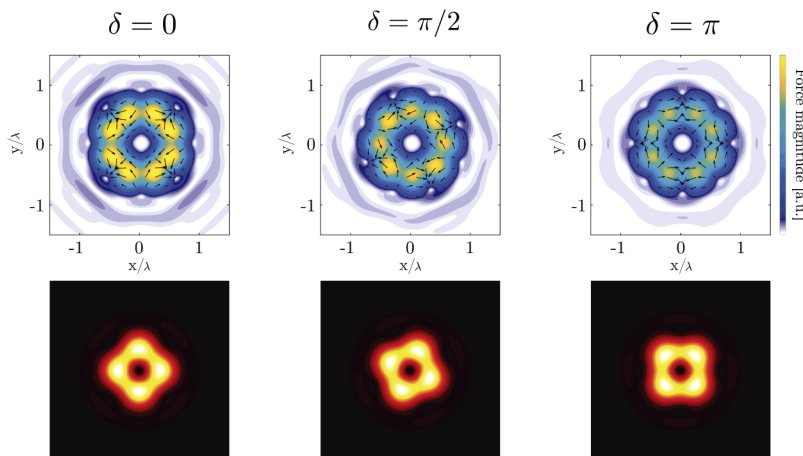


Fig. 8. Transverse optical radiation force density of a tightly focused CV beam with $\ell = -1$ for various values of $\delta = 0, \pi/2, \pi$ at the focal plane. The colormap indicates the force magnitude, whereas the arrows indicate the force direction. The lower row shows the corresponding intensity profile at the focal plane.

Finally, we completed our analysis by calculating the optically induced radiation force density for tightly focused FP beams, namely lemon and star beams. The results of numerical simulation are shown in Fig. 9. As in the case of the CV beams, the total force density preserves the symmetry exhibited by the intensity distribution of the field in the focal plane. The absorption-dependent force contribution for both cases of lemon and star topologies is formed by an as single ring, whose direction depends on the sign of η – the force is clockwise for the case of a lemon topology ($\eta = 1/2$) and counter-clockwise for the case of the star topology ($\eta = -1/2$). Notice that, for the case of the star topology, it is possible to identify four points (one is located at the centre and the other three are located around the beam centre) where the surface experiences torsion around a region of total null force.

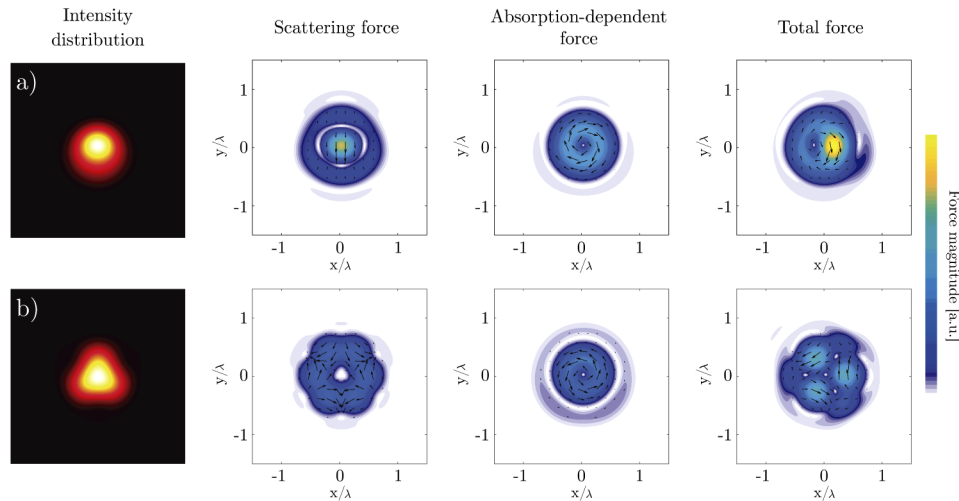


Fig. 9. Transverse optical radiation force density of a tightly FP beam for the a) lemon, and b) star polarization topologies at the focal plane. The colormap indicates the force magnitude, whereas the arrows indicate the force direction. The first column shows the corresponding intensity profile on the focal plane.

4. Conclusion

We have theoretically derived an analytical expression for the optically induced force generated by the superposition of optical vortices possessing opposite circular polarization states in the paraxial regime on a surface of an absorptive-scatter medium. We have shown the optical radiation forces for space-varying polarized optical beams, and explored the effect of the inhomogeneous polarization distribution when the intensity profile is kept invariant. In particular, for the case of a cylindrical vector beam when $\ell = 1$, it is shown that the exerted torque on the azo-polymer can be varied independently of the value of χ_i . Moreover, we have studied the induced force for three types of Full-Poincaré beams, namely lemon, star and monstar topologies. Finally, the non-paraxial case of tightly focused spatially structured polarized beams was explored numerically. It is evident that the use of spatially-variant polarised beams in the generation of much more complicated landscapes on the surface of an azo-polymer film is possible. We believe this work will be of interest in the applications of nanostructuring of azo-benzene materials, and would be of interest for exploring physics of light-matter interaction in the linear regime.

Funding

Canada Research Chairs; Ontario Early Researcher Award (ERA); Natural Sciences and Engineering Research Council of Canada.

Acknowledgements

The authors would like to thank Alicia Sit and Hugo Larocque for fruitful discussions and thoughtful feedback. This work was supported by Canada Research Chairs (CRC), Ontario's Early Researcher Award (ERA), and Natural Sciences and Engineering Research Council (NSERC).

Disclosures

The authors declare that there are no conflicts of interest related to this article.

References

1. H. Rubinsztein-Dunlop, A. Forbes, M. V. Berry, M. R. Dennis, D. L. Andrews, M. Mansuripur, C. Denz, C. Alpmann, P. Banzer, T. Bauer, E. Karimi, L. Marrucci, M. Padgett, M. Ritsch-Marte, N. M. Litchinitser, N. P. Bigelow, C. Rosales-Guzmán, A. Belmonte, J. P. Torres, T. W. Neely, M. Baker, R. Gordon, A. B. Stilgoe, J. Romero, A. G. White, R. Fickler, A. E. Willner, G. Xie, B. McMorrán, and A. M. Weiner, "Roadmap on structured light," *J. Opt.* **19**(1), 013001 (2017).
2. S. Franke-Arnold, L. Allen, and M. Padgett, "Advances in optical angular momentum," *Laser Photonics Rev.* **2**(4), 299–313 (2008).
3. R. Chen, K. Agarwal, C. J. Sheppard, and X. Chen, "Imaging using cylindrical vector beams in a high-numerical-aperture microscopy system," *Opt. Lett.* **38**(16), 3111–3114 (2013).
4. K. Zhanghao, X. Chen, W. Liu, M. Li, Y. Liu, Y. Wang, S. Luo, X. Wang, C. Shan, H. Xie, J. Gao, X. Chen, D. Jin, X. Li, Y. Zhang, Q. Dai, and P. Xi, "Super-resolution imaging of fluorescent dipoles via polarized structured illumination microscopy," *Nat. Commun.* **10**(1), 4694 (2019).
5. B. Ndagano, I. Nape, M. A. Cox, C. Rosales-Guzman, and A. Forbes, "Creation and detection of vector vortex modes for classical and quantum communication," *J. Lightwave Technol.* **36**(2), 292–301 (2017).
6. A. E. Willner, H. Huang, Y. Yan, Y. Ren, N. Ahmed, G. Xie, C. Bao, L. Li, Y. Cao, Z. Zhao, J. Wang, M. P. J. Lavery, M. Tur, S. Ramachandran, A. F. Molisch, N. Ashrafi, and S. Ashrafi, "Optical communications using orbital angular momentum beams," *Adv. Opt. Photonics* **7**(1), 66–106 (2015).
7. G. Gibson, J. Courtial, M. J. Padgett, M. Vasnetsov, V. Pas'ko, S. M. Barnett, and S. Franke-Arnold, "Free-space information transfer using light beams carrying orbital angular momentum," *Opt. Express* **12**(22), 5448–5456 (2004).
8. J. Wang, J.-Y. Yang, I. M. Fazal, N. Ahmed, Y. Yan, H. Huang, Y. Ren, Y. Yue, S. Dolinar, M. Tur, and A. E. Willner, "Terabit free-space data transmission employing orbital angular momentum multiplexing," *Nat. Photonics* **6**(7), 488–496 (2012).
9. F. Bouchard, A. Sit, F. Hufnagel, A. Abbas, Y. Zhang, K. Heshami, R. Fickler, C. Marquardt, G. Leuchs, R. W. Boyd, and E. Karimi, "Quantum cryptography with twisted photons through an outdoor underwater channel," *Opt. Express* **26**(17), 22563–22573 (2018).
10. M. Erhard, R. Fickler, M. Krenn, and A. Zeilinger, "Twisted photons: new quantum perspectives in high dimensions," *Light: Sci. Appl.* **7**(3), 17146 (2018).
11. V. Garcés-Chávez, D. McGloin, H. Melville, W. Sibbett, and K. Dholakia, "Simultaneous micromanipulation in multiple planes using a self-reconstructing light beam," *Nature* **419**(6903), 145–147 (2002).
12. F. G. Mitri, R. X. Li, L. X. Guo, and C. Y. Ding, "Optical tractor Bessel polarized beams," *J. Quant. Spectrosc. Radiat. Transfer* **187**, 97–115 (2017).
13. J. Baumgartl, M. Mazilu, and K. Dholakia, "Optically mediated particle clearing using Airy wavepackets," *Nat. Photonics* **2**(11), 675–678 (2008).
14. S. Zhang, J. Zhou, and Y.-X. Ren, "Ray optics analysis of optical forces on a microsphere in a $(2 + 1)$ D Airy beam," *OSA Continuum* **2**(2), 378–388 (2019).
15. F. G. Mitri, "Pulling and spinning reversal of a subwavelength absorptive sphere in adjustable vector Airy light-sheets," *Appl. Phys. Lett.* **110**(18), 181112 (2017).
16. L. Wang, "Optical forces on submicron particles induced by full Poincaré beams," *Opt. Express* **20**(19), 20814–20826 (2012).
17. M. F. Ferrer-García and D. Lopez-Mago, "Newtonian orbits of nanoparticles interacting with structured light beams," *J. Opt.* **21**(12), 125403 (2019).
18. M. Alameer, A. Jain, M. G. Rahimian, H. Larocque, P. B. Corkum, E. Karimi, and V. R. Bhardwaj, "Mapping complex polarization states of light on a solid," *Opt. Lett.* **43**(23), 5757–5760 (2018).

19. M. G. Rahimian, F. Bouchard, H. Al-Khazraji, E. Karimi, P. B. Corkum, and V. R. Bhardwaj, "Polarization dependent nanostructuring of silicon with femtosecond vortex pulse," *APL Photonics* **2**(8), 086104 (2017).
20. F. Takahashi, K. Miyamoto, H. Hidai, K. Yamane, R. Morita, and T. Omatsu, "Picosecond optical vortex pulse illumination forms a monocrystalline silicon needle," *Sci. Rep.* **6**(1), 21738 (2016).
21. F. Takahashi, S. Takizawa, H. Hidai, K. Miyamoto, R. Morita, and T. Omatsu, "Optical vortex pulse illumination to create chiral monocrystalline silicon nanostructures," *Phys. Status Solidi A* **213**(4), 1063–1068 (2016).
22. K. Toyoda, F. Takahashi, S. Takizawa, Y. Tokizane, K. Miyamoto, R. Morita, and T. Omatsu, "Transfer of light helicity to nanostructures," *Phys. Rev. Lett.* **110**(14), 143603 (2013).
23. X. Wang, *Azo Polymers: Synthesis, Functions and Applications*, Soft and Biological Matter (Springer-Verlag, 2017), 1st ed.
24. D. Kim, S. Tripathy, L. Li, and J. Kumar, "Laser-induced holographic surface relief gratings on nonlinear optical polymer films," *Appl. Phys. Lett.* **66**(10), 1166–1168 (1995).
25. P. Rochon, E. Batalla, and A. Natansohn, "Optically induced surface gratings on azoaromatic polymer films," *Appl. Phys. Lett.* **66**(2), 136–138 (1995).
26. S. Bian, J. M. Williams, D. Y. Kim, L. Li, S. Balasubramanian, J. Kumar, and S. Tripathy, "Photoinduced surface deformations on azobenzene polymer films," *J. Appl. Phys.* **86**(8), 4498–4508 (1999).
27. S. Bian, L. Li, J. Kumar, D. Kim, J. Williams, and S. Tripathy, "Single laser beam-induced surface deformation on azobenzene polymer films," *Appl. Phys. Lett.* **73**(13), 1817–1819 (1998).
28. M. Watabe, G. Juman, K. Miyamoto, and T. Omatsu, "Light induced conch-shaped relief in an azo-polymer film," *Sci. Rep.* **4**(1), 4281 (2015).
29. A. Ambrosio, L. Marrucci, F. Borbone, A. Roviello, and P. Maddalena, "Light-induced spiral mass transport in azo-polymer films under vortex-beam illumination," *Nat. Commun.* **3**(1), 989 (2012).
30. K. Masuda, R. Shinozaki, Y. Kinezuka, J. Lee, S. Ohno, S. Hashiyada, H. Okamoto, D. Sakai, K. Harada, K. Miyamoto, and T. Omatsu, "Nanoscale chiral surface relief of azo-polymers with nearfield oam light," *Opt. Express* **26**(17), 22197–22207 (2018).
31. D. Barada, G. Juman, I. Yoshida, K. Miyamoto, S. Kawata, S. Ohno, and T. Omatsu, "Constructive spin-orbital angular momentum coupling can twist materials to create spiral structures in optical vortex illumination," *Appl. Phys. Lett.* **108**(5), 051108 (2016).
32. Y. Nakata, M. Yoshida, and N. Miyanaga, "Parallel fabrication of spiral surface structures by interference pattern of circularly polarized beams," *Sci. Rep.* **8**(1), 13448 (2018).
33. S. Hvilsted, C. Sánchez, and R. Alcalá, "The volume holographic optical storage potential in azobenzene containing polymers," *J. Mater. Chem.* **19**(37), 6641–6648 (2009).
34. M.-S. Ho, A. Natansohn, C. Barrett, and P. Rochon, "Azo polymers for reversible optical storage. 8. the effect of polarity of the azobenzene groups," *Can. J. Chem.* **73**(11), 1773–1778 (1995).
35. M.-S. Ho, A. Natansohn, and P. Rochon, "Azo polymers for reversible optical storage. 9. copolymers containing two types of azobenzene side groups," *Macromolecules* **29**(1), 44–49 (1996).
36. S. L. Oscurato, M. Salvatore, F. Borbone, P. Maddalena, and A. Ambrosio, "Computer-generated holograms for complex surface reliefs on azopolymer films," *Sci. Rep.* **9**(1), 6775 (2019).
37. Q. Zhan, "Cylindrical vector beams: from mathematical concepts to applications," *Adv. Opt. Photonics* **1**(1), 1 (2009).
38. A. M. Beckley, T. G. Brown, and M. A. Alonso, "Full Poincaré beams," *Opt. Express* **18**(10), 10777–10785 (2010).
39. V. Lucarini, K.-E. Peiponen, J. J. Saarinen, and E. M. Vartiainen, *Kramers-Kronig Relations in Optical Materials Research*, Springer Series in Optical Sciences 110 (Springer-Verlag, 2005), 1st ed.
40. I. Freund, "Polarization singularity indices in Gaussian laser beams," *Opt. Commun.* **201**(4-6), 251–270 (2002).
41. J. F. Nye, *Natural focusing and fine structure of light: caustics and wave dislocations* (CRC, 1999).
42. B. Khajavi and E. J. Galvez, "High-order disclinations in space-variant polarization," *J. Opt.* **18**(8), 084003 (2016).
43. B. Richards, E. Wolf, and D. Gabor, "Electromagnetic diffraction in optical systems, ii. structure of the image field in an aplanatic system," *Proc. R. Soc. Lond. A* **253**(1274), 358–379 (1959).
44. T. Bauer, P. Banzer, E. Karimi, S. Orlov, A. Rubano, L. Marrucci, E. Santamato, R. W. Boyd, and G. Leuchs, "Observation of optical polarization Möbius strips," *Science* **347**(6225), 964–966 (2015).
45. T. Bauer, P. Banzer, F. Bouchard, S. Orlov, L. Marrucci, E. Santamato, R. W. Boyd, E. Karimi, and G. Leuchs, "Multi-twist polarization ribbon topologies in highly-confined optical fields multi-twist polarization ribbon topologies in highly-confined optical fields," *New J. Phys.* **21**(5), 053020 (2019).
46. E. Otte, K. Tekce, and C. Denz, "Tailored intensity landscapes by tight focusing of singular vector beams," *Opt. Express* **25**(17), 20194 (2017).
47. L. Novotny and B. Hecht, *Principles of nano-optics* (Cambridge University, 2012), 2nd ed.
48. K. Y. Bliokh, E. A. Ostrovskaya, M. A. Alonso, O. G. Rodríguez-Herrera, D. Lara, and C. Dainty, "Spin-to-orbital angular momentum conversion in focusing, scattering, and imaging systems," *Opt. Express* **19**(27), 26132–26149 (2011).